HHS Public Access

Author manuscript

Nat Chem Biol. Author manuscript; available in PMC 2019 September 04.

Published in final edited form as:

Nat Chem Biol. 2019 April ; 15(4): 377–383. doi:10.1038/s41589-019-0240-7.

Potassium channel selectivity filter dynamics revealed by single-molecule FRET

Shizhen Wang[1,2,*], **Sun-Joo Lee**[1], **Grigory Maksaev**[1], **Xin Fang**[1], **Chong Zuo**[1], and **Colin G. Nichols**[1,*]

[1]Center for Investigation of Membrane Excitability Diseases, Department of Cell Biology and Physiology, Washington University School of Medicine, St. Louis Missouri, USA

[2]Division of Cell Biology and Biophysics, School of Biological Sciences, University of Missouri-Kansas City, Kansas City, Missouri, USA

Abstract

Potassium (K) channels exhibit exquisite selectivity for conduction of K^+ ions over other cations, particularly Na^+. High resolution structures reveal an archetypal selectivity filter (SF) conformation in which dehydrated K^+, but not Na^+, ions are perfectly coordinated. Using single molecule FRET (smFRET), we show that the SF-forming loop (SF-loop) in KirBac1.1 transitions between constrained and dilated conformations as a function of ion concentrations. The constrained conformation, essential for selective K^+ permeability, is stabilized by K^+ but not Na^+ ions. Mutations that render channels non-selective result in dilated and dynamically unstable conformations, independent of the permeant ion. Further, while wild type KirBac1.1 channels are K^+-selective in physiological conditions, Na^+ permeates in the absence of K^+. Moreover, while K^+ gradients preferentially support $^{86}Rb^+$ fluxes, Na^+ gradients preferentially support $^{22}Na^+$ fluxes. This suggests differential ion selectivity in constrained versus dilated states, potentially providing a structural basis for this anomalous mole fraction effect.

Graphical Abstract

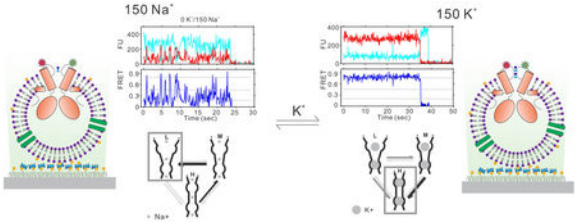

*Corresponding author – Colin. Nichols (cnichols@wustl.edu), or Shizhen Wang (wangshizhen@umkc.edu).

Author contributions

S.W. and C.G.N. conceived and designed the studies; S.W. performed smFRET experiments and fluorescence flux assays with help from C.Z.; S.J.L. performed radioactive rubidium flux assays; S.W. and S.J.L. analyzed data with help from X.F., G.M. and C.G.N. S.W. and C.G.N. prepared the manuscript with editing input from other authors.

Competing Financial Interests

We declare that none of the authors have competing financial or non-financial interests as defined by Nature Research.

Non-technical summary:

Electrical activity of living cells, as underlies neuronal and cardiac function, for instance, depends on selective permeation of charged ions across cell membranes. Central to this process, potassium channels exhibit an exquisite sensitivity for permeating potassium ions over sodium ions. Crystallographic and cryo-electron microscopy studies show a specific structural conformation in the channel pore that accommodates potassium ions but not sodium ions. By visualizing movements within individual channel proteins, we show that rather than being pre-formed, this specific structure is actually stabilized by potassium ions themselves. This helps explain how the structure is so perfectly arranged to accommodate potassium ions and not other ions.

Introduction

Selective permeation of potassium (K^+) ions at near diffusion limited rates, through membrane proteins known as potassium (K) channels, is fundamental to the development of cellular membrane potentials, and is essential for control of the intracellular ionic milieu, electrical activity, and life itself[1]. The highly conserved K channel selectivity filter (SF) discriminates K^+ over other cations, particularly Na^{+1}. High resolution crystal structures of multiple K^+ channels all reveal a common SF structure that forms multiple sites which coordinate K^+, and through which K^+ ions process in single file[2–4]. The polarity, size and geometry of these K^+ binding sites mimic those of the water dipoles that coordinate K^+ ions in solution, thermodynamically favoring the binding of K^+ over Na^+. Selective conduction of K^+ is then proposed to result from a 'knock-on' mechanism, whereby entering ions destabilize the next ion in the file[5–9]. Central to this proposed mechanism of selective conductance is that the SF must maintain a relatively fixed conformation in order to maintain optimal coordination of K^+ ions. However, we have little insight as to how or whether or how such a conformation would be maintained without the coordinated K^+ ions being present, and there have been no direct observations of the temporal dynamics of the SF. There are many reports that the SF 'collapses' into an inactivated state in the absence of K^+ ions[10–12], the reversibility of which is not always clear. There have been few reports of successful crystallization of potassium-selective channels in pure Na^+-containing solutions to provide a view of the structural correlates, and no experimental approaches to assessing the dynamics of such processes.

Results

smFRET reveals ion-dependent SF-loop dynamics

We recently developed a single-molecule FRET approach to permit real time assessment of conformational dynamics in the inward rectifier K channel KirBac1.1 embedded in a lipid membrane (Supplementary Fig. 1a)[13]. In that first study we reported a constrained conformation of the SF-loop, demonstrated by stable, high (~0.8) FRET efficiencies between fluorophores placed at diagonal T120C sites of the homotetrameric channel (Fig. 1a)[13]. That study was carried out in the presence of 150 mM [K^+], which generates high K^+ occupancies within the SF[14]. However, even in these conditions, some channels occasionally transit to low FRET efficiency conformations. We speculate that these transitions might be

related to changes in SF conformation, and might be affected by K^+ ion occupancies. To investigate this possibility further, we have examined conformational dynamics of the SF-loop in the complete absence of K^+ (replaced with 150 mM Na^+). Strikingly, under these conditions, the SF-loop FRET signals are no longer predominantly high FRET efficiencies, but switch predominantly to additional low (~0.2) and medium (~0.45) FRET efficiencies with frequent transitions between them (Fig. 1a, *top*). Although we cannot discount the possibility that such distinct FRET efficiencies actually represent states of different fluorophore mobility, T120C residues are well exposed and, therefore, the attached fluorophores are likely to adopt random orientations and conform to $\kappa^2 = 2/3$ (see Discussion). With this assumption, the predicted distances of FRET 0.8, 0.45 and 0.2 efficiency states are 40, 52 and 64 Å. The highest (0.8) FRET efficiency-predicted distance being very close to that predicted by KirBac1.1 crystal structure (PDB 1P7B, 36 Å for T120 Cα-Cα distance, obtained in high [K^+]), while the FRET 0.45 and 0.2 state could represent dilation (i.e. outward movement from the pore axis) of one or both of the diagonally labeled subunits, respectively, although the structural motion required (~10 Å in each subunit) is several-fold bigger than that typically suggested by 'collapsed' or 'flipped' structures of the SF reported in crystal structures or in dynamic simulations.

Over the whole range of [K^+], the FRET amplitude distributions (Supplementary Fig. 1b) show clear peaks, requiring a minimum sum of 3 Gaussians for adequate fitting (Supplementary Fig. 1b), with FRET peaks at 0.2, 0.45 and 0.8. Addition of low concentrations of K^+ in the presence of 150 mM Na^+ results in a dramatic concentration-dependent change in dynamic behaviors at the SF-loop, which switch from being dilated and dynamic back to being compact and relatively stable, above ~1mM K^+ (Fig. 1b). Occupancy of the intermediate FRET state (FRET ~0.45) shows a shallow dependence on [K^+], with a peak at ~1 mM [K^+], while relative occupancies of the low and high FRET states decrease or increase, respectively, with apparent K_d of ~1 mM and Hill coefficient (nH) of ~0.5 (Fig. 1c). This is similar to the concentration-dependence of K^+ ion binding in the SF obtained using other approaches[15,16].

In contrast to the marked ion-dependence of FRET signals at residue T120C, the FRET distributions and dynamics at residue A45C, which is located in the cytoplasmic slide helix region, are insensitive to switching from 150 mM K^+ to 150 mM Na^+ (Fig. 1d). This important control data set indicates that the channel complex remains intact in the latter condition and, moreover, that conformational effects of K^+ are local to the SF region and are not propagated through the channel complex. Interestingly, although the stable high FRET state predominates at what would be physiological external [K^+] of 5 mM (Fig. 1b), dynamic transitions to intermediate and low FRET states are still clearly detectable. Zhou et al[3] previously suggested that SF structural transitions between 'conducting' and non-conducting' states should occur under physiological conditions, but were unable to detect them in crystal or Cryo-EM structures. We confirmed that spontaneous SF conformational transitions do occur under physiological ionic conditions by immobilizing KirBac1.1 proteoliposomes asymmetrically, such that the 'cytoplasmic' domain of the channel faces 145 mM [K^+], while the extracellular side of the channel faces 5 mM [K^+] (Fig. 1e).

[K^+]-dependent conformational kinetics

The [K^+]-dependence of FRET amplitude distributions (Fig. 1c) suggests a simple scenario in which the SF-loop of the two diagonally apposed subunits contributing to the FRET signal are predominantly dilated away from the pore axis (generating the low FRET0.2 state, L), or in intermediate position (the intermediate FRET0.45 state, M), or constricted towards the pore axis (the high FRET0.8 state, H). To gain further insight to potential kinetic schemes that might account for the observed transitions, we have analyzed the kinetics of idealized concatenated FRET records (Fig. 2a, Supplementary Fig. 2, see Methods). In general, individual trajectories are dominated by single FRET states within the available duration of the FRET recording. In 150 mM [K^+], ~92% of traces exhibit high FRET states, and only 6.8% of traces exhibit single, low FRET states. In 150 mM [Na^+], only ~15% traces exhibit stable high FRET states, and in these conditions, only ~10% and 8% of traces, respectively, exhibit all three FRET states, due to the limiting lifetime of single molecule FRET imaging. We considered any traces exhibiting 2 or 3 distinct FRET states as dynamic traces, the percentage of dynamic traces for 0, 0.005, 0.05, 0.5, and 150 mM [K^+] were 42, 54, 44, 51, 47 and 35%, respectively. To overcome the limitations of short recordings and attempt to estimate lifetimes, we randomly concatenated all trajectories obtained under the same condition[17] (see Methods). This analysis indicates that lifetime distributions are generally exponential, and that mean FRET lifetimes increase for the H state as [K^+] increases, and M state lifetimes show bell-shaped dependence on [K^+], although there is no obvious decline in mean lifetime for the L state (Fig. 2b). Not only lifetimes, but also transition paths, are obtained from such idealizations, allowing calculation of individual rate constants for each transition (Fig. 2c, see Methods). This analysis indicates that increase in the M>H and L>H transition rates, and decrease in the M>L transition rate, are the predominant drivers of altered FRET distributions as [K^+] increases, with relatively [K^+] independent L>M, H>L and H>M transitions (Fig. 2c). We considered whether an allosteric 3-state kinetic model, in which transition rate constants depend on [K^+], might suffice to explain the FRET distributions and transition kinetics. Such a model (see Supplementary Fig. 3a,b), in which transition rate constants and [K^+]-dependence were manually adjusted (but constrained to maintain micro-reversibility, Fig. 2b), readily accounts for the distribution of FRET amplitudes (Supplementary Fig. 3c, *left*). However, it does not fully account for the measured [K^+]-dependent lifetimes (Supplementary Fig. 3c, *right*), although we note that given the limitation of short time recordings, lifetimes are likely to be underestimated, even after concatenation.

Pore blocking ions also control SF dynamics

Tetra-alkylammonium compounds (e.g. TEA^+ and THA^+) mimic hydrated K^+ ions and are classical blockers of K channels, including Kir channels[14–20], binding at the extracellular or intracellular entrances to the channel[20–21]. We examined the effects of TEA^+ and THA^+ on SF-loop FRET signals, in the presence of 0.5 mM K^+/150 mM Na^+. Even at this low [K^+], the stable high FRET conformation otherwise predominates (Fig. 1b), but addition of either TEA^+ (Fig. 3a) or THA^+ (Supplementary Fig. 4a) causes a dramatic shift of the FRET distribution to low and medium FRET states. The apparent Kd values are ~0.5 mM for TEA^+ (Fig. 3b) and ~0.05 mM for THA^+ (Supplementary Fig. 4b), close to those obtained for TEA^+ and THA^+ block of K channels in electrophysiological studies[20,22]. In crystal

structures of KcsA complexed with TEA^+ (extracellular side) or THA^+ (inner cavity side), K^+ occupancies are decreased at the inner (S2, S3) binding sites but are increased at outer sites (S1, S4) [20,21]. We thus suggest that the striking TEA^+ and THA^+ de-stabilization of the constrained SF-loop conformation may reflect decreased K^+ ion occupancy of deep sites within the SF itself.

$NMDG^+$ is a large organic cation that is sterically excluded from the selective ion binding sites in K channels. Neither addition of $NMDG^+$ on the 150 mM Na^+ background, nor of Na^+ on a 150 mM $NMDG^+$ background, affected the SF-loop conformation (Supplementary Fig. 5). However, when K^+ ions were introduced on the 150 mM $NMDG^+$ background, restoration of the constrained conformation again occurred (Fig. 3c), but with a higher affinity and steeper $[K^+]$-dependence compared to K^+ addition to 150 mM Na^+ (Fig. 3d), consistent with functional and structural findings that Na^+, but not $NMDG^+$, may compete for SF binding sites when K^+ ions are present within the SF[23,24].

Ion-independent SF-loop dynamics in non-selective mutants

The signature amino acid sequence 'TxGYG' within the K channel SF-loop generates the canonical K^+ binding sites and is highly conserved throughout the K channel superfamily[25] (Supplementary Fig. 6). As shown in Fig. 4a, specific mutations in the signature sequence that can abolish K^+ selectivity (as first identified in the voltage-dependent Shaker K channel[26]), also abolish K^+ selectivity of KirBac1.1 when introduced at the equivalent residues. Critically, these mutations also all lead to highly dynamic 120C FRET efficiencies that are insensitive to the ionic conditions (Fig. 4b,c). These results strikingly demonstrate that loss of K^+-selectivity is coupled to loss of K^+-dependent stability of the SF-loop conformation. These results thus provide consistency with the idea that the constrained high FRET state, K^+-selective SF-loop conformation, rather than being a pre-existing state, is actually maintained by K^+ ion-SF interactions. This is in turn consistent with biochemical demonstration that, in SDS, K^+ ions control quaternary stability of KcsA[15] and KirBac1.1 channels[27].

The mechanism of K-selectivity

Highly selective K^+ permeation through K channels requires preferential binding of K^+ ions over Na^+ ions in the channel SF. The above results imply that the SF conformation is itself dependent on the ions that are present. This has important additional implications regarding ion permeation through the channel. First, the dilated, dynamic, SF conformations that we observe in pure Na^+ solutions are time-stable within the time course of our experiments and are fully reversible upon re-addition of K^+ ions. They therefore do not reflect an irreversibly collapsed filter state, and raises the possibility that these conformations might actually be Na^+ permeating states. We tested this directly by examining ion fluxes into KirBac1.1-containing liposomes, under driving forces generated solely by Na^+ or by K^+ ions (Fig. 5a,b). Robust Na^+-driven Na^+ fluxes are clearly detectable in KirBac1.1, implying that the dilated SF conformation can accommodate and permeate Na^+ ions (Fig. 5a,b). Importantly, we also detect $^{22}Na^+$ fluxes when the driving force is generated by K^+ ions, but these K^+-driven $^{22}Na^+$ fluxes are actually smaller than Na^+-driven fluxes (Fig. 5a). Since the channel is highly K^+ (or Rb^+)-selective under physiological conditions[28,29], it is unlikely that the

driving membrane voltage is lower with K^+-driven fluxes, further suggesting that K^+ ions actually inhibit Na^+ flux. Conversely, K^+-driven Rb^+ fluxes are much higher than Na^+-driven Rb^+-fluxes (Fig. 5b). This then suggests that $^{22}Na^+$ fluxes are lower when K^+ ions provide the driving force (and generate the constrained conformation) because Na^+ actually permeates the dilated SF conformation, rather than, or at least better than, it does the K^+-selective, constrained, conformation.

Discussion

We have visualized conformational dynamics of the KirBac1.1 channel SF-loop using smFRET. Our results indicate that the SF-loop is stabilized in a constrained, high FRET conformation by high [K^+], but becomes conformationally more dynamic, with frequent transitions between lower FRET conformations, at low or zero [K^+]. Conformational flexibility of the SF has been reported using solid state NMR previously[30,31], but the relevance has not been fully clear and has not been examined at the single molecule level, nor with the temporal and conformational resolution that our studies provide. A major role for K^+ ion binding in maintaining stability of the entire channel tetramer has been shown in detergent-solubilized K channels[15,27,32], suggesting that, in the absence of K^+ ions, the canonical SF structure is at least less stable. The notion of a relatively fixed K channel SF conformation has been repeatedly cautioned against by computational models of SF dynamics [33–38]. Importantly, the present results do not support an ion-independent pore conformation, and are therefore difficult to reconcile with previous crystallographic studies which have suggested a stably canonical K channel SF conformation, even in the absence of Na^+ [39]. It is conceivable that crystal constructs help to stabilize the constrained, canonical conformation in such experiments. Here we provide experimental evidence for conformational dynamics of the SF-loop in the presence of Na^+ or impermeant organic cations, and stabilization in a high FRET conformation by high concentrations of K^+ ions. Kinetic analysis indicates that the rate of transitions into the constrained high FRET state are increased by K^+, and transitions out of this state are decreased by K^+. This is consistent with preferentially K^+ ion binding sites being generated in this state, and in turn suggests that selectivity for K^+ against Na^+ may originate with the inability of Na^+ ions to stabilize the backbone carbonyls of the SF-loop in the necessary tetrameric conformation that selectively permits efficient K^+ diffusion across the membrane.

Although we do not interpret FRET efficiencies in terms of absolute distances, it is important to consider whether the FRET efficiencies we observe are feasible, given the known features of the channel structure. We assessed predicted FRET efficiencies using the FRET-restrained Positioning and Screening (FPS) software package[40] for the KirBac1.1 crystal structure (2WLL) obtained in high KCl conditions (>50 mM). FPS analysis indicates full fluorophore accessibility to a cone-like space centered at T120, supporting assumption of 2/3 for the orientation factor (Supplementary Fig. 7). The predicted average donor-acceptor distance is 52±11 Å, and predicted mean FRET efficiency is ~0.48. Our smFRET measurements indicate 3 predominant FRET efficiencies (0.8, 0.45, 0.2), with average FRET 0.62 in high [K^+]. This is higher than the FPS-predicted average FRET 0.48, but a significant portion of the calculated accessible volume extends into the space which is presumed to be occupied by membrane (Supplementary Fig. 7). As a result, the real

accessible volume and the average donor-acceptor distances may be over-estimated by the FPS software package. With the above assumptions, the lowest (0.2) amplitude FRET conformation we report would imply significant ~10 Å increase in the residue 120 Cα-Cα separation. However, we cannot assess the degree of anisotropy in our measurements, and increased anisotropy in the lowest amplitude FRET conformations could result in the above distance changes being overestimated. Nevertheless, we note that in the HCN channel structure[41], which contains a GYG SF-filter but is non-selective, the Cα-Cα distance between diagonal residues at the external glycine is at least 10 Å wider than in the K^+-selective KcsA[41]. Potentially the low FRET states we observe reflect similar structural conformations.

Our results demonstrate marked, ion-dependent, conformational dynamics in the potassium channel extracellular region. They lead us to conclude that selective K^+ or Rb^+ permeation is achieved primarily by the stabilization of the constrained, high FRET (K^+ conducting) state by ion-channel interactions. Similarly, the dynamic, low FRET state might be specifically stabilized by interactions with other (i.e. Na^+) ions, potentially generating a Na^+ conducting state, and explaining why Na^+ permeation is inhibited by K^+ ions, and *vice versa* K^+ permeation is inhibited by Na^+ ions (Fig. 5). Such an ‘anomalous mole fraction effect’ has been detected in many ion channels, including Ca^+-activated and Na^+-conducting K^+ channels, as well as Ca^{2+} channels[39,42,43]. The prevailing explanation involves the interaction of ions of different species with one another inside an implicitly fixed conformation multi-ion pore but, as has been explicitly acknowledged, changing the mole fraction of two permeant ions (e.g. K^+ and Na^+) “might alter the fraction of time that the channel exists in conformations of different permeability[1]”.

Online Methods

a. Plasmids

Plasmids containing tandem dimeric KirBac1.1 protein-encoding cDNAs (A45C-WT, T120C-WT) were constructed in previous studies using the pQE60 expression vector (Amp^r)[13,28]. For KirBac1.1 non-selective mutants, mutations were introduced by QuikChange II XL site-directed mutagenesis kit (Agilent Inc.) and confirmed by DNA sequencing.

b. Protein expression, purification and fluorophore labeling

Tandem dimeric KirBac1.1 (WT and mutant) proteins were expressed and purified following protocols reported previously[13,27]. The metal affinity-purified proteins were passed through a Superdex-200 10/300 size exclusion column (GE Healthcare Inc.) with running buffer containing 20 mM Hepes, 150 mM KCl, 5 mM DM, pH7.0. Tetrameric fractions were pooled and concentrated via Amicon Ultra-4 centrifugal filter (MWCO 100 KDa, Millipore Inc.). Fluorophore labeling was started immediately after gel filtration by adding 1:1 (molar ratio) mix of Alexa Fluor 555 and 647 c2 maleimide to protein solution at final protein:fluorophore molar ratio of 1:5. Labeling reactions proceeded at room temperature for 1 hr and were then terminated by addition of 2-mercaptoethanol at final concentration of 10 mM. A second metal affinity purification was performed to remove free fluorophores or

those associated with protein through non-covalent bonds. The labeled proteins were loaded onto a size exclusion column (Superdex-200 10/300, GE Healthcare Inc) and tetrameric fractions were collected and concentrated for liposome reconstitution. A labeling control using KirBac1.1 WT protein with no intrinsic cysteine was always included to evaluate fluorophores bound non-specifically or associated with protein through non-covalent bonds. All purifications were performed at 4°C except for labeling reactions.

c. Protein reconstitution

POPE and POPG lipids (3:1, w/w) were dissolved in buffer containing 20 mM Hepes, 150 mM KCl and 30 mM CHAPS, pH 7.5, at final concentration of 10 mg/ml. Protein labeled with Alexa Fluor 555 and 647 fluorophores was mixed with lipid solution at protein:lipid ratio of 1:200 (w/w), with or without 2% biotinylated-POPE (w/w, of the total lipids), depending on the sample immobilization configuration. The lipid/protein mix was incubated at room temperature for 20 min then passed through a sephadex G-50 desalting column to remove detergents, thereby forming proteoliposomes. Residual detergents were removed by dialysis against 1 L buffer containing 20 mM Hepes, 150 mM KCl, pH7.5 for 2 times and proteoliposomes were harvested and stored at −80 °C freezer for single molecule imaging.

d. Single molecule imaging

Chamber slides were prepared following the protocol of Joo et al[44]. An objective-based TIRF microscope, built on a Nikon inverted microscope (TE-2000s) with 100x APO TIRF NA1.49 objective lens, 532 nm and 640 nm lasers, was used for single molecule imaging. Donor and acceptor emissions were separated by OptoSplit II (Cairn Inc.) with 638 nm longpass beam splitter, passed through 585/65 nm and 700/75 nm emission filters (Chroma Inc.) and then collected by Evolve 512 delta EMCCD camera (Photometrics Inc.). A CRISP auto focus system (ASI Inc.) was incorporated to compensate focus drift due to mechanical vibrations and thermo fluctuations. Liposomes containing fluorophore-labeled KirBac1.1 proteins were immobilized on the slide surface by biotin-neutravidin interactions either with biotinylated-POPE in liposomes or biotin conjugated monoclonal anti-His-tag antibodies (1:200 dilution, ThermoFisher Inc.). Fluorophores were excited by 532 nm laser and movies were collected using NIS-element (Nikon Inc) with frame rates of 10 per second (i.e. time resolution of 100 ms). Laser power was ~ 9.1 W/cm^2 (at the objective lens side). Recording times were typically <3 min, with half bleaching times typically ~45 sec. Except for the 20 mM Hepes and different concentrations of cations, all imaging buffers contained ~3 mM Trolox, 2 mM NBA, 2 mM COT, 5 mM PCA and 15 μg/μL of PCD to enhance the photostability of the fluorophores[45,46]. 50 μM β-escine to permeabilize liposomes[47] was omitted for experiments with asymmetric ionic conditions. Control liposomes reconstituted with labeled control KirBac1.1 WT protein at the same concentration were included to evaluate the fluorescent impurities, ensuring that they were less than 5%, in comparison with sample liposomes. For every protein, at least 2 independent labeled samples were used; for every sample, at least 6 movies were collected.

e. Single molecule imaging data analysis

For every movie, there were typically, 400–600 molecules per field of view with ~80 molecules containing both acceptor and donor fluorophores. Individual molecules were

identified and donor and acceptor fluorescence intensity profiles were extracted by IDL scripts developed by the Ha group[48,49]. Leak and direct excitation corrections were not applied, since leakage was lower than 0.06 and direct excitation was essentially undetectable. Traces were inspected and selected manually following criteria described in previous publications[13,50]. The bin size of all time histograms was set at 0.02x recording time, ensuring equal contribution from each trace to avoid dominant effects of long traces[17]. FRET contour plots were generated from the first 3 s data from each trace. For idealizing smFRET traces using Clampfit software, FRET levels were updated independently with level contribution as 5% and 'Ignore short level changes' and 'Latency Mode' disabled. Traces in the same condition were concatenated into a single file[17]. The number of transitions in each records was usually >>5x the number of 'stitched' records, and false transitions at stitch points were ignored.

f. Fluorescence liposome flux assay

KirBac1.1 proteins were reconstituted into POPE/POPG liposomes with protein:lipid ratio of 1:500, by passing through Sephadex G-50 desalting columns equilibrated with buffer 20 mM Hepes, 150 mM KCl, pH7.5. Immediately before flux assay, the extraliposomal buffer was replaced by buffers containing different concentration of counter cations, such as LiCl, NaCl, KCl, RbCl and CsCl and the total external cation concentration was adjusted to 150 mM by adding NMDG·HCl. ACMA stock was then added to reach a final concentration of 13 μM and liposomes loaded into a 96-well plate. Baseline fluorescence (excitation wavelength 400/30 nm and emission wavelength 495/10 nm, Top50 Mirror) were measured by a Synergy 2 plate reader. After 3 min, CCCP stock was added by the Synergy2 injection system to final concentration of 3.2 μM and the ACMA fluorescence was monitored continuously with the same setting for 25 min. The ionic flux was evaluated by ACMA fluorescence quenching with the following equation:

$$\text{Flux} = (Fb - Fa) / Fb$$

Where Fb and Fa are the average fluorescence intensities of the sample before, and 20 min after, adding CCCP. All flux data were normalized to the flux with no external counter cations.

g. Radioactive rubidium and sodium flux assays

KirBac1.1 proteins were reconstituted and $^{86}Rb^{+}$ and $^{22}Na^{+}$ flux assays were performed as described previously[27].

h. Kinetic modeling

FRET kinetics and amplitude distributions were examined using a simple 3-state kinetic model in which the transition rates (k) between states were dependent on occupancy by K^{+} ions according to the following equation:

$$k = k_{zero} + k_{diff}(K_D^{nH} / (1 + K_D^{nH}),$$

where k_{zero} = rate constant in zero K^+, k_{diff} = change in k at saturating [K^+], and nH = Hill coefficient.

i. Statistics

The FRET histogram data of each sample/condition was presented as mean ± s.e.m. with equal contribution from all individual traces (rather than each data point). The FRET contour map for each sample/condition was calculated from the first 3 s of all traces, with equal contribution from all individual traces (all selected traces were longer than 5 secs). The trace number n for each sample/condition is included in the accompanying figure legends.

Data Availability and Code Availability Statements

Data collection is described in the Online Methods. Source codes are also listed.Software for initial data processing was IDL scripts developed by the Ha group (fully described in refs 48,49), and available upon request. Subsequent analysis was carried out using Clampfit v7.0 and in Microsoft Excel.

Supplementary Material

Refer to Web version on PubMed Central for supplementary material.

Acknowledgements

The work was funded by NIH grant R35 HL140024 to CGN.

Abbreviations:

FRET:	fluorescence resonance energy transfer
TIRFM	total internal reflection fluorescence microscope
NMDG	n-methyl-D-glucamine
POPE	1-palmitoyl-2-oleoyl-sn-glycero-3-phosphoethanolamine
POPG	1-palmitoyl-2-oleoyl-*sn*-glycero-3-phospho-(1'-*rac*-glycerol)
Trolox	6-hydroxy-2,5,7,8-tetramethylchroman-2-carboxylic acid
NBA	4-nitrobenzyl alcohol
COT	cyclooctatetraene
PCA	protocatechuic acid
PCD	protocatechuate-3,4-dioxygenase
ACMA	9-amino-6-chloro-2-methoxyacridine
CCCP	carbonyl cyanide m-chlorophenyl hydrazine
TEA	tetraethylammonium

THA	tetrahexylammonium

References,Methods only references

1. Hille B Ion channels of excitable membranes, xviii, 814 p. (Sinauer, Sunderland, Mass, 2001).
2. Doyle DA et al. The structure of the potassium channel: molecular basis of K+ conduction and selectivity. Science 280, 69–77 (1998). [PubMed: 9525859]
3. Zhou Y, Morais-Cabral JH, Kaufman A & MacKinnon R Chemistry of ion coordination and hydration revealed by a K+ channel-Fab complex at 2.0 A resolution. Nature 414, 43–8 (2001). [PubMed: 11689936]
4. Varma S, Rogers DM, Pratt LR & Rempe SB Perspectives on: ion selectivity: design principles for K+ selectivity in membrane transport. The Journal of general physiology 137, 479–88 (2011). [PubMed: 21624944]
5. Roux B Ion conduction and selectivity in K(+) channels. Annual review of biophysics and biomolecular structure 34, 153–71 (2005).
6. Berneche S & Roux B Energetics of ion conduction through the K+ channel. Nature 414, 73–7 (2001). [PubMed: 11689945]
7. Aqvist J & Luzhkov V Ion permeation mechanism of the potassium channel. Nature 404, 881–4 (2000). [PubMed: 10786795]
8. Noskov SY, Berneche S & Roux B Control of ion selectivity in potassium channels by electrostatic and dynamic properties of carbonyl ligands. Nature 431, 830–4 (2004). [PubMed: 15483608]
9. Shrivastava IH, Tieleman DP, Biggin PC & Sansom MS K(+) versus Na(+) ions in a K channel selectivity filter: a simulation study. Biophysical journal 83, 633–45 (2002). [PubMed: 12124253]
10. Wang W & MacKinnon R Cryo-EM Structure of the Open Human Ether-a-go-go-Related K(+) Channel hERG. Cell 169, 422–430 e10 (2017). [PubMed: 28431243]
11. Cuello LG, Jogini V, Cortes DM & Perozo E Structural mechanism of C-type inactivation in K(+) channels. Nature 466, 203–8 (2010). [PubMed: 20613835]
12. Labro AJ, Cortes DM, Tilegenova C & Cuello LG Inverted allosteric coupling between activation and inactivation gates in K(+) channels. Proceedings of the National Academy of Sciences of the United States of America 115, 5426–5431 (2018). [PubMed: 29735651]
13. Wang S, Vafabakhsh R, Borschel WF, Ha T & Nichols CG Structural dynamics of potassium-channel gating revealed by single-molecule FRET. Nature structural & molecular biology 23, 31–6 (2016).
14. Zhou Y & MacKinnon R The occupancy of ions in the K+ selectivity filter: charge balance and coupling of ion binding to a protein conformational change underlie high conduction rates. Journal of molecular biology 333, 965–75 (2003). [PubMed: 14583193]
15. Krishnan MN, Bingham JP, Lee SH, Trombley P & Moczydlowski E Functional role and affinity of inorganic cations in stabilizing the tetrameric structure of the KcsA K+ channel. The Journal of general physiology 126, 271–83 (2005). [PubMed: 16129774]
16. Lockless SW, Zhou M & MacKinnon R Structural and thermodynamic properties of selective ion binding in a K+ channel. PLoS biology 5, e121 (2007). [PubMed: 17472437]
17. Blanco M & Walter NG Analysis of complex single-molecule FRET time trajectories. Methods in enzymology 472, 153–78 (2010). [PubMed: 20580964]
18. Guo D, Ramu Y, Klem AM & Lu Z Mechanism of rectification in inward-rectifier K+ channels. The Journal of general physiology 121, 261–75 (2003). [PubMed: 12642596]
19. Guo D & Lu Z Kinetics of inward-rectifier K+ channel block by quaternary alkylammonium ions. dimension and properties of the inner pore. The Journal of general physiology 117, 395–406 (2001). [PubMed: 11331349]
20. Lenaeus MJ, Burdette D, Wagner T, Focia PJ & Gross A Structures of KcsA in complex with symmetrical quaternary ammonium compounds reveal a hydrophobic binding site. Biochemistry 53, 5365–73 (2014). [PubMed: 25093676]
21. Lenaeus MJ, Vamvouka M, Focia PJ & Gross A Structural basis of TEA blockade in a model potassium channel. Nature structural & molecular biology 12, 454–9 (2005).

22. Thompson J & Begenisich T Affinity and location of an internal K+ ion binding site in shaker K channels. The Journal of general physiology 117, 373–84 (2001). [PubMed: 11331347]
23. Thompson AN et al. Mechanism of potassium-channel selectivity revealed by Na(+) and Li(+) binding sites within the KcsA pore. Nature structural & molecular biology 16, 1317–24 (2009).
24. Sauer DB, Zeng W, Canty J, Lam Y & Jiang Y Sodium and potassium competition in potassium-selective and non-selective channels. Nature communications 4, 2721 (2013).
25. McCoy JG & Nimigean CM Structural correlates of selectivity and inactivation in potassium channels. Biochimica et biophysica acta 1818, 272–85 (2012). [PubMed: 21958666]
26. Heginbotham L, Lu Z, Abramson T & MacKinnon R Mutations in the K+ channel signature sequence. Biophysical journal 66, 1061–7 (1994). [PubMed: 8038378]
27. Wang S, Alimi Y, Tong A, Nichols CG & Enkvetchakul D Differential roles of blocking ions in KirBac1.1 tetramer stability. The Journal of biological chemistry 284, 2854–60 (2009). [PubMed: 19033439]
28. Enkvetchakul D et al. Functional characterization of a prokaryotic Kir channel. The Journal of biological chemistry 279, 47076–80 (2004). [PubMed: 15448150]
29. Cheng WW, Enkvetchakul D & Nichols CG KirBac1.1: it's an inward rectifying potassium channel. The Journal of general physiology 133, 295–305 (2009). [PubMed: 19204189]
30. Lange A et al. Toxin-induced conformational changes in a potassium channel revealed by solid-state NMR. Nature 440, 959–62 (2006). [PubMed: 16612389]
31. Bhate MP, Wylie BJ, Tian L & McDermott AE Conformational dynamics in the selectivity filter of KcsA in response to potassium ion concentration. Journal of molecular biology 401, 155–66 (2010). [PubMed: 20600123]
32. Krishnan MN, Trombley P & Moczydlowski EG Thermal stability of the K+ channel tetramer: cation interactions and the conserved threonine residue at the innermost site (S4) of the KcsA selectivity filter. Biochemistry 47, 5354–67 (2008). [PubMed: 18419132]
33. Roux B et al. Ion selectivity in channels and transporters. The Journal of general physiology 137, 415–26 (2011). [PubMed: 21518830]
34. Roux B Ion channels and ion selectivity. Essays in biochemistry 61, 201–209 (2017). [PubMed: 28487397]
35. Nimigean CM & Allen TW Origins of ion selectivity in potassium channels from the perspective of channel block. The Journal of general physiology 137, 405–13 (2011). [PubMed: 21518829]
36. Dixit PD & Asthagiri D Thermodynamics of ion selectivity in the KcsA K+ channel. The Journal of general physiology 137, 427–33 (2011). [PubMed: 21518831]
37. Alam A & Jiang Y Structural studies of ion selectivity in tetrameric cation channels. The Journal of general physiology 137, 397–403 (2011). [PubMed: 21518828]
38. Andersen OS Perspectives on: Ion selectivity. The Journal of general physiology 137, 393–5 (2011). [PubMed: 21518827]
39. Ye S, Li Y & Jiang Y Novel insights into K+ selectivity from high-resolution structures of an open K+ channel pore. Nature structural & molecular biology 17, 1019–23 (2010).
40. Kalinin S et al. A toolkit and benchmark study for FRET-restrained high-precision structural modeling. Nat Methods 9, 1218–25 (2012). [PubMed: 23142871]
41. Lee CH & MacKinnon R Structures of the Human HCN1 Hyperpolarization-Activated Channel. Cell 168, 111–120 e11 (2017). [PubMed: 28086084]
42. Kiss L, Immke D, LoTurco J & Korn SJ The interaction of Na+ and K+ in voltage-gated potassium channels. Evidence for cation binding sites of different affinity. The Journal of general physiology 111, 195–206 (1998). [PubMed: 9450939]
43. Almers W & McCleskey EW Non-selective conductance in calcium channels of frog muscle: calcium selectivity in a single-file pore. The Journal of physiology 353, 585–608 (1984). [PubMed: 6090646]
44. Joo C & Ha T Preparing sample chambers for single-molecule FRET. Cold Spring Harbor protocols 2012, 1104–8 (2012). [PubMed: 23028078]

45. Aitken CE, Marshall RA & Puglisi JD An oxygen scavenging system for improvement of dye stability in single-molecule fluorescence experiments. Biophysical journal 94, 1826–35 (2008). [PubMed: 17921203]

46. Dave R, Terry DS, Munro JB & Blanchard SC Mitigating unwanted photophysical processes for improved single-molecule fluorescence imaging. Biophysical journal 96, 2371–81 (2009). [PubMed: 19289062]

47. Fan JS & Palade P Perforated patch recording with beta-escin. Pflugers Archiv : European journal of physiology 436, 1021–3 (1998). [PubMed: 9799421]

48. Roy R, Hohng S & Ha T A practical guide to single-molecule FRET. Nature methods 5, 507–16 (2008). [PubMed: 18511918]

49. Joo C & Ha T Single-molecule FRET with total internal reflection microscopy. Cold Spring Harbor protocols 2012(2012).

50. Wang S, Brettmann JB & Nichols CG Studying Structural Dynamics of Potassium Channels by Single-Molecule FRET in Potassium Channels 163–180 (Springer, 2018).

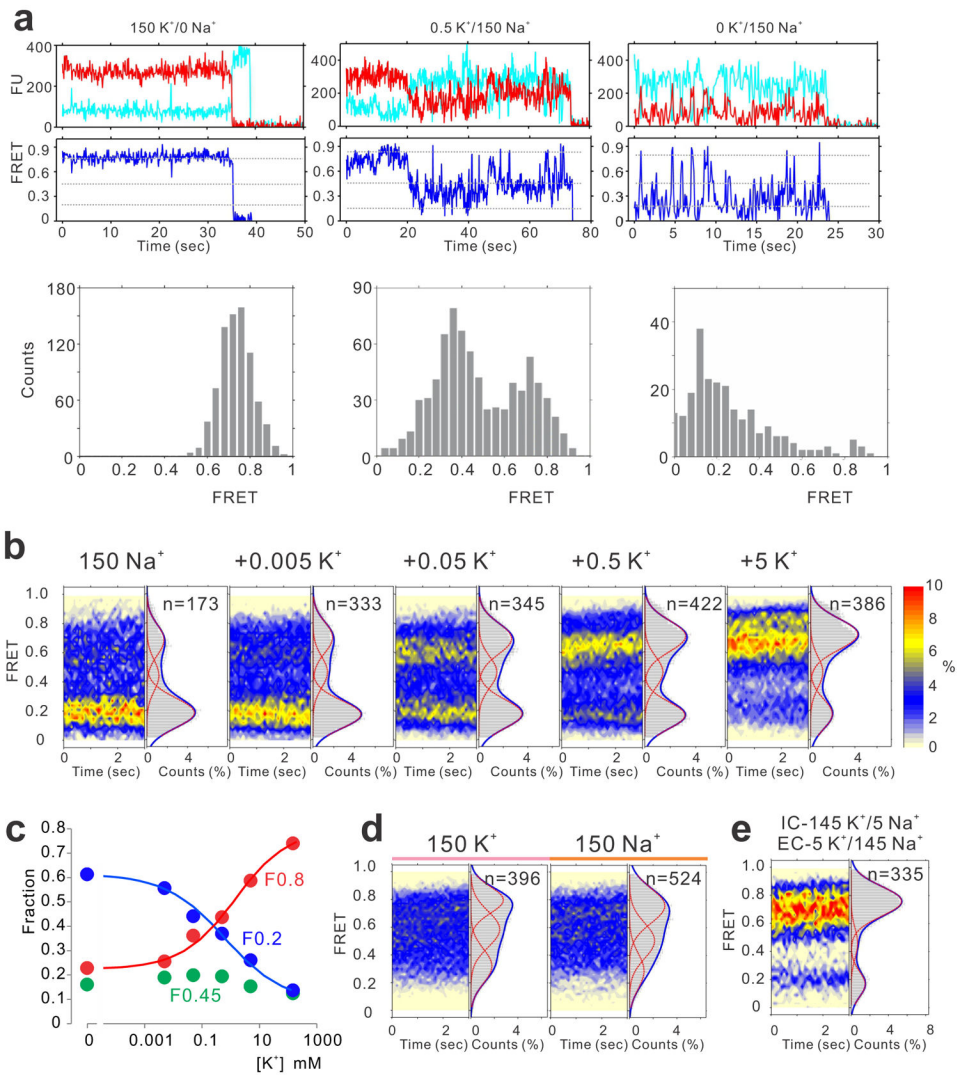

Fig. 1. The SF-loop conformation is dependent on ion occupancies

a. Representative smFRET trajectories (above) and associated FRET amplitude histograms (below) at T120C sites under different ionic conditions as indicated. Fluorescence intensities of the donor Alexa Fluor 555 and acceptor Alexa Fluor 647 are colored cyan and red, respectively, FRET is colored blue. The FRET levels 0.2, 0.45 and 0.8 are marked by dashed lines. **b.** FRET contour maps and histograms for AF555/647 fluorophores labeled at diagonal T120C sites in the SF-loop, at increasing [K^+] from 0–5 mM, on a 150 mM Na^+ background, as indicated (n= 173, 333, 345, 422 and 386 traces). **c**. Fractional amplitudes from 3 state fits to FRET contour maps in b, plus Hill equation fits of [K^+] dependence of fractional occupancy of high (F0.8, red, $K_{1/2}$= 1.34 mM, nH= 0.5) and low (F0.2, blue, $K_{1/2}$= 0.69 mM, nH= 0.5) states. The amplitudes of medium (F0.45, green) FRET populations were not fitted. **d.** FRET contour maps and histograms for AF555/647 fluorophores labeled at the diagonal A45C sites in the SF-loop, in 150 mM [K^+] (n= 396 traces) or 150 mM Na^+ (n= 524 traces), as indicated. **e.** FRET contour map and histogram for AF555/647 fluorophores labeled at the diagonal T120C sites in the SF-loop in

asymmetric 145 mM [K^+] on the cytoplasmic side, while the extracellular side of the channel faces 5 mM [K^+] (n= 335 traces).

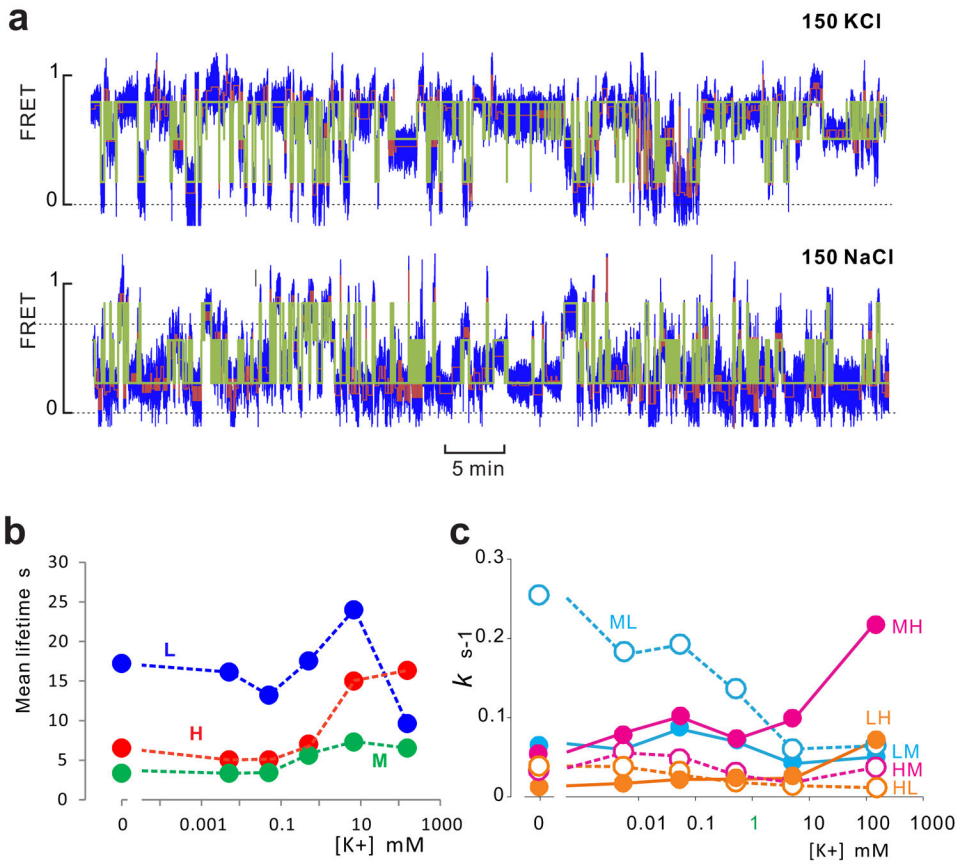

Fig. 2. Permeant ion-dependent kinetics of SF-loop conformational dynamics

a. Concatenated smFRET trajectories (blue) in 150 mM KCl (n=363 traces) and 150 mM NaCl (n= 173 traces), together with raw idealizations (brown) and subsequent cut-off idealization into low (0.2), middle (0.45) and high (0.8) FRET states (green). **b.** Mean lifetime in low (L), medium (M) and high (H) FRET states as a function of $[K^+]$, from cut-off idealization into 3 states for concatenated trajectories as in a (and Supplementary Fig. 2). **c**. Transition rate constants between L, M and H (ML is rate constant for transition from M to L, etc) as a function of $[K^+]$.

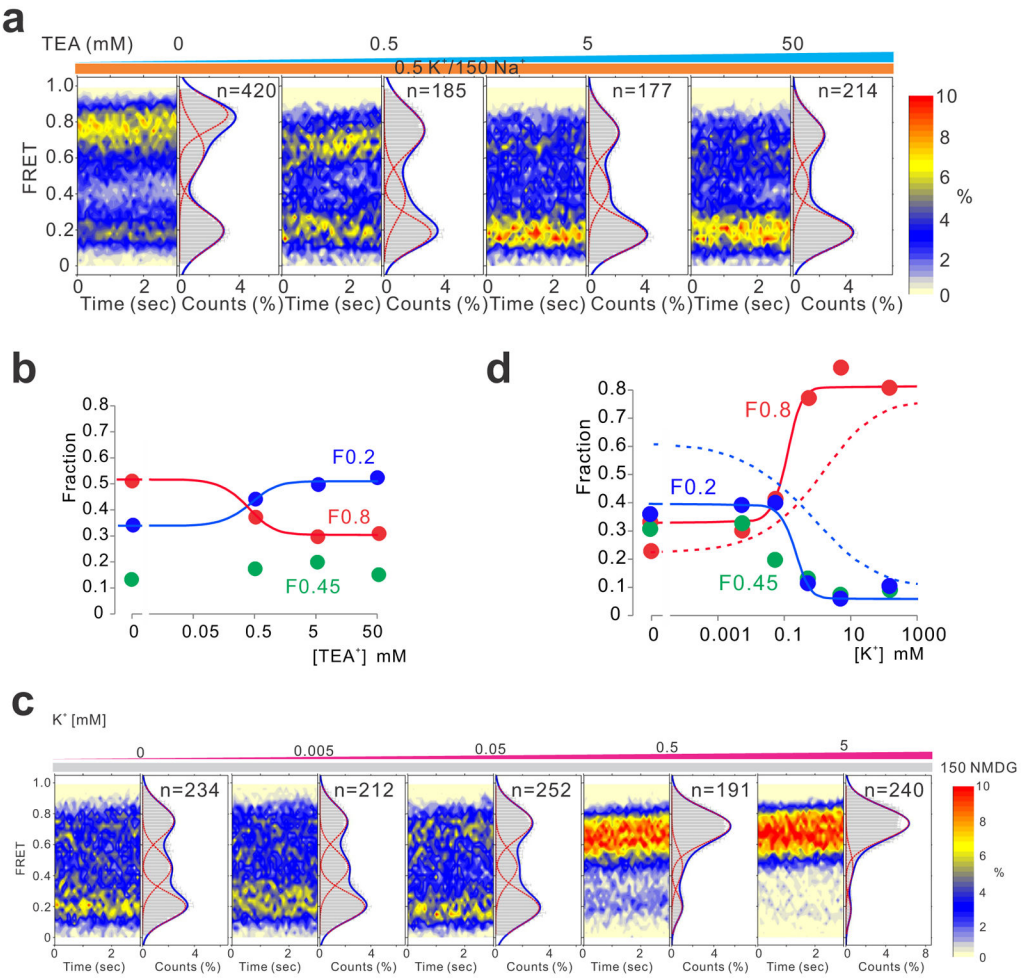

Fig. 3. Quaternary ammonium ions and impermeant NMDG stabilize low FRET states

a. FRET contour maps and histograms for AF555/647 fluorophores labeled at diagonal T120C sites of KirBac1.1 SF-loop with different concentrations of TEA^+ (n= 420, 185, 177 and 214 traces). **b**. Fractional amplitudes from 3 state fits to FRET contour maps in a. Hill equation fits of dependence of fractional occupancy of high (F0.8, red) and low (F0.2, blue) states. The amplitudes of medium (F0.45, green) FRET populations were not fitted. **c.** FRET contour maps and histograms for AF555/647 fluorophores labeled at the diagonal T120C sites in the SF-loop, with increasing $[K^+]$ from 1–5 mM, on a 150 mM $NMDG^+$ background, as indicated (n= 234, 212, 252, 191 and 240 traces). **d**. Fractional amplitudes from 3 state fits to FRET contour maps in b. Hill equation fits of $[K^+]$ dependence of fractional occupancy of high (F0.8, red, $K_{1/2}$= 0.12 mM, nH= 2.0) and low (F0.2, blue, $K_{1/2}$= 0.22 mM, nH= 2.0) states. Comparable fits for 150 mM Na^+ background (Fig. 1e) are shown as dashed lines. The amplitudes of medium (F0.45, green) FRET populations were not fitted.

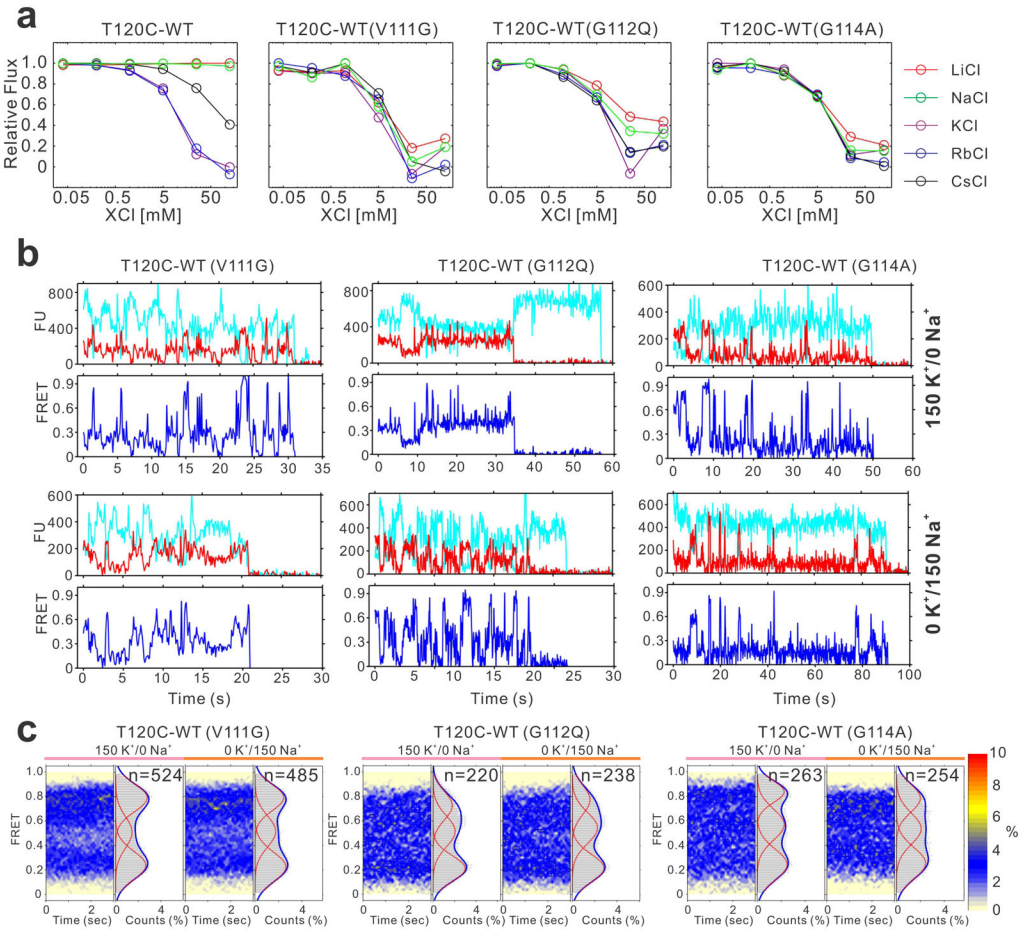

Fig. 4. Non-selective KirBac1.1 mutants exhibit dynamic conformations that are not stabilized by either K or Na.

a. Ion-selectivity of KirBac1.1 WT and mutants labeled at diagonal T120C sites with Alexa Fluor 555 and 647 fluorophores. WT channels show flux inhibition by permeant K^+, Rb^+ and Cs^+ ions but not by impermeant Na^+ or Li^+, whereas the mutant channels are inhibited by all ions. **b.** Representative smFRET trajectories at T120C sites for KirBac1.1 non-selective mutations, in 150 mM KCl or 150 mM NaCl, as indicated. Fluorescence intensities of the donor Alexa Fluor 555 and acceptor Alexa Fluor 647 are colored cyan and red, respectively, FRET is colored blue. **c.** FRET contour maps and histograms at diagonal T120C labeling sites of KirBac1.1 non-selective mutants (from left to right, n= 524, 485, 220, 238, 263 and 254 traces) in either 150 mM KCl (left) or 150 NaCl (right).

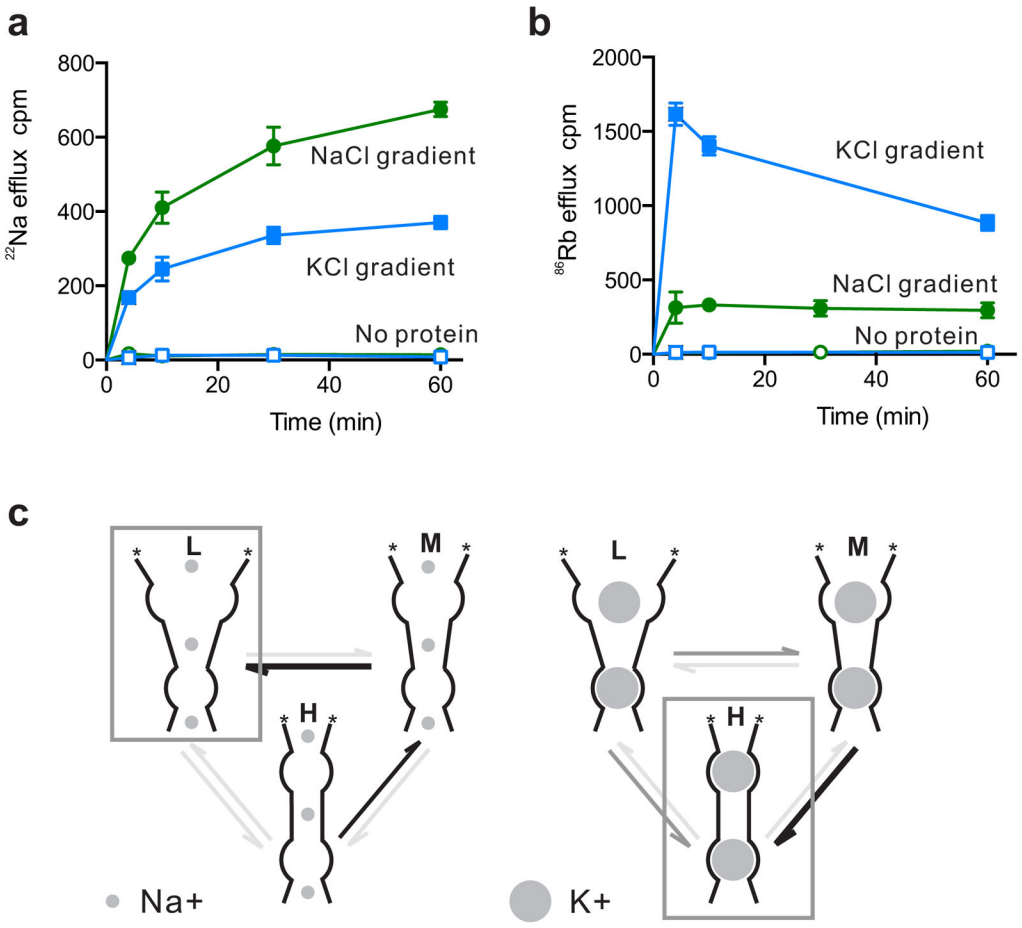

Fig. 5. Permeant ion induced conductance in KirBac1.

a, b. Time course of $^{22}Na^{+}$ (A) or $^{86}Rb^{+}$ (B) uptake into liposomes (POPE:POPG, 75: 25%), with 450 mM internal and 0.05 mM external [K^{+}] (blue), or with 450 mM internal and 0.05 mM external [Na^{+}] (green). Liposomes were reconstituted with no protein (open symbols), or with KirBac1.1 (2.5 μg/mg lipid, filled symbols), n=3 in each condition. **c**. Cartoon representation of proposed model for ion-dependent conformational transitions in KirBac1.1. The selectivity filter exists predominantly in a constrained high FRET state (H), an intermediate medium FRET state (M) or a dilated low FRET state (L). Na ions in the pore favor transitions away from the H state, particularly the H to M and M to L transitions. K^{+} ions in the pore favor transitions to the H state, in which the SF generates the 'canonical' K^{+} selective ion binding sites.